PML-FDTD Simulation for Dispersive, Inhomogeneous, and Conductive Earth

W.C. Chew[1], M. Oristaglio[2], and T. Wang[3]

[1]Center for Computational Electromagnetics
University of Illinois, Urbana, IL 61801
[2]Schlumberger-Doll Research
Old Quarry Road, Ridefield, CT 06877
[3]Western Atlas Wireline Services
10201 Westheimer, Houston, TX 77042

1. Introduction

Dispersive media are often encountered in rocks, earth and biological media [1-7]. The dispersive phenomenon can result from dielectric relaxation in the media. This could be a consequence of geometrical effect of insulating rock platelets immersed in a conductive host [6]. It could also be the result of the interaction of electromagnetic fields with the double layer around colloidal suspensions in a saline solution [7]. When the permittivity varies as a function of frequencies, the conductivity also varies as a function of frequencies as dictated by the causality requirement of the Kramers-Kronig relations [8].

Therefore, to have a realistic model of the lossy earth, it is prudent that we include the effect of dispersion in the media. For the model, we will assume either a Debye relaxation model or the Lorentzian relaxation model [9-11]. The Debye relaxation model is a special case of the Lorentzian model. Therefore, we need only to address the Lorentzian model, albeit developing a code tailored especially for the Debye model will be more efficient than a general purpose code for a general relaxation model. The model is causal so that the Kramers-Krong relationship is automatically satisfied. Because of this, the permittivity value will be complex having both a frequency dependent real and imaginary parts. The imaginary part can be thought of as frequency-dependent loss or conductivity.

We will use the recursive convolution approach [9-11] for modeling a dispersive medium and using the split Maxwell's equations with PML as the absorbing boundary condition [12-14] to simulate an infinite conductive region.

As will be noted, the modeling of the dispersive, conductive media comes not without a cost. More storage and computation is needed in order to model the conductive dispersive media appropriately.

2. PML-FDTD Formulation

The PML can be related to a complex coordinates stretching in the frequency domain [14]. This is necessitated by a splitting of Maxwell's equations in the time domain. This splitting generally doubles the memory requirements of an FDTD simulation. When conductive loss is added, this further increases the memory requirements because of an added conductivity term in the PML equation. We will see that the inclusion of dispersion further increases the memory requirement.

The stretched coordinates Maxwell's equations are

$$\nabla_s \times \mathbf{E} = i\omega\mathbf{B}, \tag{1}$$

$$\nabla_s \times \mathbf{H} = -i\omega\mathbf{D} + \sigma\mathbf{E}, \tag{2}$$

for a conductive medium in the frequency domain with $e^{-i\omega t}$ dependent. In the above

$$\nabla_s = \hat{x}\frac{1}{s_x}\partial_x + \hat{y}\frac{1}{s_y}\partial_y + \hat{z}\frac{1}{s_z}\partial_z, \tag{3}$$

where s_x, s_y, and s_z are frequency dependent complex stretching variables. To facilitate the solution in the time domain, (1) and (2) are usually split as follows:

$$i\omega \mathbf{B}_{sx} = \frac{1}{s_x}\partial_x \hat{x} \times \mathbf{E}, \tag{4}$$

$$-i\omega \mathbf{D}_{sx} + \sigma \mathbf{E}_{sx} = \frac{1}{s_x}\partial_x \hat{x} \times \mathbf{H}, \tag{5}$$

where the same is repeated for y and z replacing x.

By letting $s_x = a_x + i\frac{\Omega_x}{\omega}$, where a_x and Ω_x are frequency independent, the above becomes

$$i\omega a_x \mathbf{B}_{sx} - \Omega_x \mathbf{B}_{sx} = \partial_x \hat{x} \times \mathbf{E}, \tag{6}$$

$$-i\omega a_x \mathbf{D}_{sx} + \Omega_x \mathbf{D}_{sx} + a_x \sigma \mathbf{E}_{sx} + i\frac{\Omega_x}{\omega}\sigma \mathbf{E}_{sx} = \partial_x \hat{x} \times \mathbf{H}_{sx}. \tag{7}$$

Transforming the above back into the time domain, one obtains

$$-a_x \partial_t \mathbf{B}_{sx} - \Omega_x \mathbf{B}_{sx} = \partial_x \hat{x} \times \mathbf{E}, \tag{8}$$

$$a_x \partial_t \mathbf{D}_{sx} + \Omega_x \mathbf{D}_{sx} + a_x \sigma \mathbf{E}_{sx} + \Omega_x \sigma \int_0^t \mathbf{E}_{sx}(\tau)\, d\tau = \partial_x \hat{x} \times \mathbf{H}. \tag{9}$$

In the above, for a dispersive medium, we let $\mathbf{B}_{sx} = \mu \mathbf{H}_{sx}$ while

$$\mathbf{D}_{sx}(t) = \epsilon(t) * \mathbf{E}_{sx}(t). \tag{10}$$

3. Recursive Convolution

A Lorentzian dispersive medium is characterized by [11]

$$\chi(t) = \sum_{p=1}^{P} \gamma_p e^{-\alpha_p t} \sin(\beta_p t) u(t), \tag{11}$$

where

$$\beta_p = \sqrt{\omega_p^2 - \alpha_p^2}, \tag{12}$$

$$\gamma_p = \frac{\omega_p^2 G_p(\epsilon_s - \epsilon_\infty)}{\sqrt{\omega_p^2 - \alpha_p^2}}, \tag{13}$$

and

$$\sum_{p=1}^{P} G_p = 1,$$

$$\epsilon(t) = \epsilon_0 \left[\epsilon_\infty + \chi(t)\right]. \tag{14}$$

We can define a complex susceptibility

$$\hat{\chi}(t) = \sum_{p=1}^{P} i\gamma_p e^{(-\alpha_p - i\beta_p)t} u(t), \tag{15}$$

so that $\chi(t) = \Re e[\hat{\chi}(t)]$. Note that Debye relaxation is the special case where $\beta_p = 0$, and $i\gamma_p$ is real or when $\gamma_p > \omega_p$. The electric flux is related to the electric field via

$$\mathbf{D}(t) = \epsilon_0 \epsilon_\infty \mathbf{E}(t) + \epsilon_0 \chi(t) * \mathbf{E}(t). \tag{16}$$

Using (15) in (16), we have

$$\mathbf{D}(t) = \epsilon_0 \epsilon_\infty \mathbf{E}(t) + \epsilon_0 \sum_{p=1}^{P} \Re e\big[\hat{\chi}(t) * \mathbf{E}(t)\big]. \tag{17}$$

When $t = l\Delta_t$, the above becomes

$$\mathbf{D}^l = \epsilon_0 \epsilon_\infty \mathbf{E}^l + \epsilon_0 \sum_{p=1}^{P} \Re e\big[\hat{\chi}_p^0 \mathbf{Q}_p^l\big], \tag{18}$$

where

$$\mathbf{Q}_p^l = \sum_{m=0}^{l-1} \mathbf{E}^{l-m} e^{(-\alpha_p - i\beta_p)m\Delta_t}, \tag{19}$$

$$\mathbf{Q}_p^l = \begin{cases} 0, & l = 0 \\ \mathbf{E}^l + \mathbf{Q}_p^{l-1} e^{-i\tilde{\omega}_p \Delta_t}, & l > 0 \end{cases}, \tag{20}$$

and $\tilde{\omega}_p = \beta_p - i\alpha_p$.

The above equations allow the computation of $\mathbf{D}^l$ given $\mathbf{E}^l$ as the input. However, one would like to compute $\mathbf{E}^l$ given $\mathbf{D}^l$ as the input in an FDTD scheme as we shall see later. To this end, we substitute (20) into (18) to obtain

$$\mathbf{D}^l = \epsilon_0 \left(\epsilon_\infty + \sum_{p=1}^{P} \Re e\left[\hat{\chi}_p^0\right] \right) \mathbf{E}^l + \epsilon_0 \sum_{p=1}^{P} \Re e\left[\hat{\chi}_p^0 \mathbf{Q}_p^{l-1} e^{-i\tilde{\omega}_p \Delta_t}\right], \tag{21}$$

or that

$$\mathbf{D}^l = \epsilon_0 \left(\alpha \mathbf{E}^l + \mathbf{P}^{l-1}\right), \tag{22a}$$

where

$$\alpha = \epsilon_\infty + \sum_{p=1}^{P} \Re e[\hat{\chi}_p^0], \tag{22b}$$

$$\mathbf{P}^{l-1} = \sum_{p=1}^{P} \Re e\left(\hat{\chi}_p^0 \mathbf{Q}_p^{l-1} e^{-i\tilde{\omega}_p \Delta_t}\right), \tag{22c}$$

depends only on $\mathbf{Q}_p^{l-1}$.

4. The Time-Stepping Scheme

We need to devise a time-stepping scheme for Equations (8) and (9). The space discretization is done according to the Yee scheme [15] so that we will not discuss it here. The time discretization for them are as follows:

$$\frac{-a_x\left(\mathbf{B}_{sx}^{l+\frac{1}{2}} - \mathbf{B}_{sx}^{l-\frac{1}{2}}\right)}{\Delta_t} - \Omega_x \mathbf{B}_{sx}^{l+\frac{1}{2}} = \partial_x \hat{x} \times \mathbf{E}^l, \tag{23}$$

$$\frac{a_x\left(\mathbf{D}_{sx}^{l+1}-\mathbf{D}_{sx}^{l}\right)}{\Delta_t}+\Omega_x\mathbf{D}_{sx}^{l+1}+a_x\sigma\mathbf{E}_{sx}^{l+1}+\sigma\Omega_x\mathbf{F}_{sx}^{l}=\partial_x\hat{x}\times\mathbf{H}^{l+\frac{1}{2}}, \tag{24}$$

where $\mathbf{F}(t)=\int_0^t\mathbf{E}(\tau)\,d\tau$. Equation (23) can be easily rearranged for time stepping

$$\mathbf{B}_{sx}^{l+\frac{1}{2}}=-(a_x+\Omega_x\Delta_t)^{-1}\left[\Delta_t\left(\partial_x\hat{x}\times\mathbf{E}^{l}\right)-a_x\mathbf{B}_{sx}^{l-\frac{1}{2}}\right], \tag{25}$$

$$(a_x+\Omega_x\Delta_t)\mathbf{D}_{sx}^{l+1}+a_x\sigma\Delta_t\mathbf{E}_{sx}^{l+1}=\Delta_t\left(\partial_x\hat{x}\times\mathbf{H}^{l+\frac{1}{2}}\right)+a_x\mathbf{D}_{sx}^{l}-\sigma\Omega_x\Delta_t\mathbf{F}_{sx}^{l}. \tag{26}$$

However, the left-hand side of (26) depends on both $\mathbf{D}_{sx}^{l+1}$ and $\mathbf{E}_{sx}^{l+1}$ making it unsuitable for time stepping. To remove this problem, we substitute (22a) into the left-hand side of (26) so that we have

$$\begin{aligned}\left[(a_x+\Omega_x\Delta_t)\,\alpha\epsilon_0+a_x\sigma\Delta_t\right]\mathbf{E}_{sx}^{l+1}=&\Delta_t\left(\partial_x\hat{x}\times\mathbf{H}^{l+\frac{1}{2}}\right)+a_x\mathbf{D}_{sx}^{l}\\&-\sigma\Omega_x\Delta_t\mathbf{F}_{sx}^{l}-(a_x+\Omega_x\Delta_t)\epsilon_0P_{sx}^{l}.\end{aligned} \tag{27}$$

The above equation is now suitable for time stepping and updating $\mathbf{E}_{sx}^{l+1}$. After $\mathbf{E}_{sx}^{l+1}$ is updated, it is used in the right-hand side of (26) to update $\mathbf{B}_{sx}^{l+\frac{1}{2}}$ and hence $\mathbf{H}_{sx}^{l+\frac{1}{2}}$. On the right-hand side of (27), the pertinent quantities are updated as follows:

$$\mathbf{D}_{sx}^{l}=\epsilon_0\left(\alpha\mathbf{E}_{sx}^{l}+\mathbf{P}_{sx}^{l-1}\right), \tag{28a}$$

$$\mathbf{F}_{sx}^{l}=\mathbf{F}_{sx}^{l-1}+\mathbf{E}_{sx}^{l}\Delta_t, \tag{28b}$$

$$\mathbf{P}_{sx}^{l}=\sum_{p=1}^{P}\Re e\left[\hat{\chi}_p^0\mathbf{Q}_{p,sx}^{l-1}e^{-i\tilde{\omega}_p\Delta_t}\right], \tag{28c}$$

$$\mathbf{Q}_{p,sx}^{l}=\mathbf{E}_{sx}^{l}+\mathbf{Q}_{p,sx}^{l-1}e^{-i\tilde{\omega}_p\Delta t}. \tag{28d}$$

The above schemes are repeated for x replaced with y and z. Hence, (25) and (27) constitute the updating schemes for the electromagnetic fields. Storage are required for $\mathbf{H}_{s\xi}$, $\mathbf{E}_{s\xi}$, $\mathbf{F}_{s\xi}$, $\mathbf{Q}_{p,s\xi}$, $p=1,\cdots,P$, $\xi=x,y,z$ and since each $\mathbf{A}_{s\xi}$ has two vector components, we need to store $(18+6P)N$ values where N is the number of simulation nodes, and P is the number of species in the relation model. The added storage cost of simulating a PML dispersive medium is $6PN$ while the added cost of a PML conductive medium is to store $\mathbf{F}_{s\xi}$ which is $6N$. A non-dispersive, non-conductive PML medium will require $12N$ storage as opposed to the $6N$ needed in the plain Yee scheme.

5. Numerical Results

An FDTD code has been written using the above formulation. A PML medium is assumed everywhere so that the code can be easily parallelized allowing the parallel computer to work in a SIMD (single instruction multiple data) mode. The code is used to simulate the response of a vertical electric dipole on top of a half space that is dispersive and conductive.

The half space is assumed to have $\epsilon_s=50.$, $\epsilon_\infty=5.$, and a $\sigma=0.3$ mho/m. A two species Lorentz medium is assumed where $G_1=0.4$ and $G_2=1-G_1$, $f_1=2.\times10^8$, $f_2=5.\times10^8$ from which we obtain $\omega_1=2\pi f_1$ $\omega_2=2\pi f_2$. We let $\alpha_1=a_1\omega_1$ $\alpha_2=a_2\omega_2$, where $a_i<1$ for Lorentz media and $a_i>1$ for Debye media. The PML is set up with 7 parabolic-profile layers. The center frequency of the Blackman-Harris pulse is 0.5 GHz. The Courant factor is 0.8. The half space occupies 60 % of the vertical height of the cubic simulation region. The simulation is done with $50\times50\times50$ grid with a space discretization size $\Delta_s=8.47$ mm and a time step $\Delta_t=13$ ps. Assuming that the origin is at a corner of the cube, then the source is located at $\mathbf{r}_s = (0.5, 0.7, 0.5)L$, while the receive is located at $\mathbf{r}_r = (0.3, 0.5, 0.5)L$ where L is the length of the cube, which in this case is $50\Delta_s$. The receiver is deliberately buried in the half-space so that it is more sensitive to the wave propagating through the half-space.

Figure 1a and Figure 1b show the dispersive behavior of the permittivity for two Lorentz media. In Figure 1a, the $a_1 = a_2 = 0.8$ so that the Lorentz poles are quite far from the real ω axis. In this case, the two-species dispersion is not distinct. In Figure 1b, $a_1 = a_2 = 0.5$ so that the Lorentz poles are nearer to the real ω axis. One can discern distinctly two resonance peaks for this Lorentz medium. For soil, the dispersive behaviour resembles more like that of the Figure 1a.

Figure 2a shows the time response of the E_y component of the field at the receiver for the conductive medium without dispersion (solid line), with dispersion of Figure 1a (dash-dot line), and with dispersion of Figure 1b (dotted line). It is seen that the pulse is distorted to different extent by the dispersive media. The dispersive media also seems to slow down the pulse.

Figure 2b simulates the case of the dispersive media of Figure 1b for a larger number of time steps (1000) with no visible instability.

Figure 3 shows cases where the locations of the Lorentz poles are being moved by changing the Lorentz frequencies f_1 and f_2. The center frequency of the exciting pulse in this case is 1 GHz. The Lorentz frequencies are respectively, (i) $100\times$ (dashed line), (ii) $10\times$ (dotted line), (iii) the same (dash-dot line), and (iv) $0.1\times$ (heavy solid line) those shown at the begining of this section. In this case, $a_1 = a_2 = 0.5$. It is seen that different Lorentz frequencies affect the pulse propagation differently. When the exciting pulse has a center frequency close to that of the poles (case ii), the pulse is severely distorted. When the Lorentz frequencies are too high, the pulse is little affected while lower Lorentz frequencies will still distort the pulse. However, this kind of dispersive media is hardly encountered in rocks or soil.

Figure 4 shows a snap shot of the profile of the field at 1,000 time steps. It is shown that the field is well absorbed by the PML at the edge of the simulation region with no noticeable reflection or instability.

The code has been parallelized to run on a SGI Power Challenge Array. The Array has six R8000 processors running at 90 MHz. Altogether, the Array has a total of 2 GB RAM. The machine has been rated at 126 Mf/s by the Netlib Performance database. Figure 5 shows the speed of the code versus the number of processors for 100 time steps. It takes about 85 seconds to calculate 100 time steps for the aforementioned grid size with dispersion and conductive loss. The vertical axis here is the number of processors divided by the total CPU times of all the processors involved. It is noted that for a small number of processors, an almost linear speed-up is observed. When the number of processors is larger than four, the speed-up deteriorates because of contention with other ongoing codes running on the same machine.

6. Conclusions

The PML-FDTD formulation has been developed for a dispersive Lorentz medium with conductive loss. By a proper choice of the parameters, a Lorentz medium exhibits dispersions observed in some soil and rocks. It is shown that such dispersion can distort pulse shape as the pulse propagates through such a medium. It may have ramification on the design of ground penetrating radar and impulse radar for probing soil and rock formation [16].

Also, the use of the PML absorbing boundary condition allows the easy parallelization of the code compared to the use of the Liao absorbing boundary condition [17]. The stabilized Liao absorbing boundary condition generally requires double precision computation, while single precision computation suffices for PML computation. However, the use of PML in a dispersive medium comes with the added cost of more memory requirements and computational time. It is observed to take about twice as long in terms of CPU time compared to a nondispersive conductive medium calculation. A PML-conductive media modeling requires about 1.5 times the PML media modeling, while a PML-conductive-dispersive media modeling with two Lorentz species may take about 3 times the ordinary PML media modeling.

ACKNOWLEDGEMENTS

Ping Lee and Yong Hua Chen's help with the parallelization of the code is gratefully acknowledged.

REFERENCES

1. J. E. Hipp, 1974, Soil electromagnetic parameters as functions of frequency, soil density, and soil moisture:*Proc. IEEE*, **62**, 98-103.
2. W. D. Hurt, 1985, Multiterm Debye dispersion relations for permittivity of muscle: *IEEE Trans. Biomed. Eng.*, **BME-32**, 60-64.
3. D. Sullivan, 1992a, A frequency-dependent FDTD method for biological applications: IEEE Trans. Microwave Theory Tech., **40**, 532-539.
4. D. Sullivan, 1992b, Frequency-dependent FDTD methods using z transforms: IEEE Trans. Ant. Propagat., **40**, 1223-1230.
5. O. P. Gandhi, B. Q. Gao, and J. Y. Chen, 1993, A frequency-dependent finite-difference time-domain formulation for general dispersive media: *IEEE Trans. Microwave Theory Tech.*,**41**, 658-664.
6. P. N. Sen and W. C. Chew, 1983, The frequency dependent dielectric and conductivity response of sedimentary rocks, *J. Microwave Power*, **18**, no. 1, p. 95.
7. W. C. Chew and P. N. Sen, 1982, Dielectric enhancement due to electrochemical double layer: thin double layer approximation, *J. Chem. Phys.*, **77**, no. 9, p. 4683.
8. W. C. Chew, 1990, *Waves and Fields in Inhomogeneous Media,* Van Nostrand Reinhold: New York. Reprinted by IEEE Press, 1995.
9. R. Luebbers, F. P. Hunsberger, 1992, FDTD for N-th order dispersive media: *IEEE Trans. Ant. Propagat.*, **40**, 1297-1301.
10. R. Luebbers, F. P. Hunsgerger, K. S. Katz, R. B. Standler, and M. Schneider, 1990, A frequency-dependent finite-difference time-domain formulation for dispersive materials:*IEEE Trans. Electromag. Compat.,* **32**, 222-227.
11. C. M. Rappaport and W. H. Weedon, 1994, Computational issues in ground penetrating radar, unpublished report.
12. J. P. Berenger, 1994, A perfectly matched layer for the absorption of electromagnetic waves: *J. Comp. Phys.*, **114**, 185-200.
13. D. S. Katz, E. T. Thiele, and A. Taflove, 1994, Validation and extension to three dimensions of the Berenger PML absorbing boundary condition for FD-TD meshes: *IEEE Microwave and Guided Wave Lett.*, **4**, 268-270.
14. W. C. Chew and W. H. Weedon, 1994, A 3D perfectly matched medium from modified Maxwell's equations with stretched coordinates:*Micro. Opt. Tech. Lett.*,**7**, 599-604.
15. K. S. Yee, 1966, Numerical solution of initial boundary value problems involving Maxwell's equation in isotropic media: *IEEE Trans. Antennas Propagat.*, **AP-14**, 302–307.
16. M. Moghaddam, E. J. Yannakakis, W. C. Chew, and C. Randall, C., 1991, Modeling of the subserface interface radar: J. Electromag. Waves App., **5**, 17-39.
17. Z. P. Liao, H. L. Wong, B. P. Yang, and Y. F. Yuan, 1984, A transmitting boundary for transient wave analysis:*Scientia Sinca*, **27A**, 1063-1076

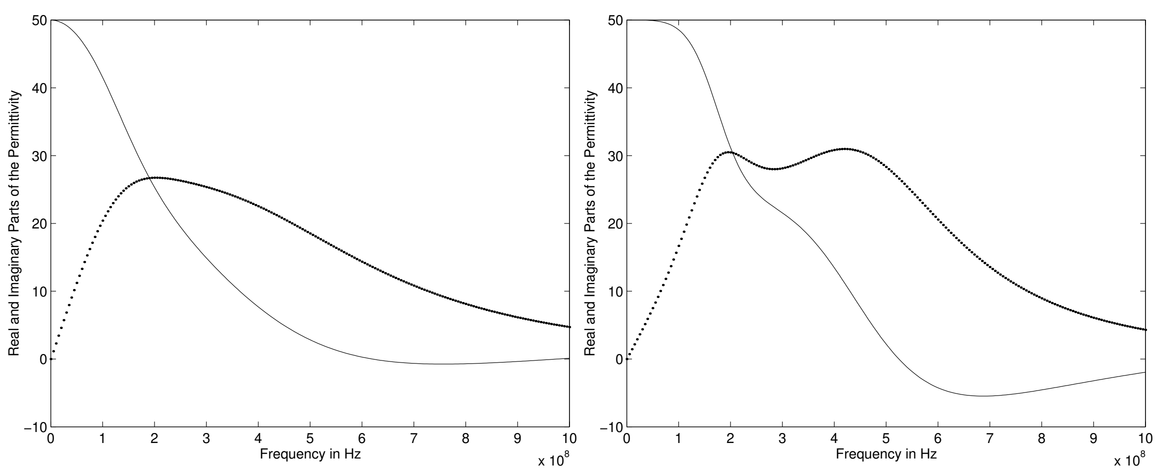

(a) **(b)**

Figure 1. Permittivity dispersion for a two species Lorentz medium with (a) $a_1 = a_2 = 0.8$. See text for more details, (b) $a_1 = a_2 = 0.5$. In this case, the poles are closer to the real ω axis, and two distinct resonances are observable.

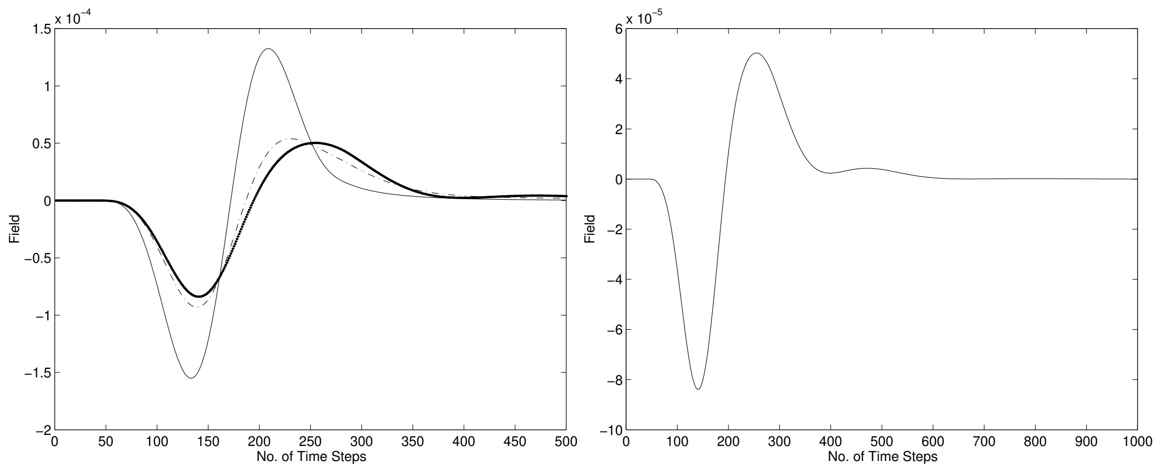

(a) **(b)**

Figure 2. (a) Pulse distortion for different Lorentz medium with conductivity loss. (i) No dispersion (solid line), (ii) dispersion with the case of Figure 1a (dash-dot line), and (iii) dispersion with the case of Figure 1b (heavy dotted line). See text for more details. (b) Same as case (iii) of (a), but run for 1000 time steps. No reflection and instability are visible.

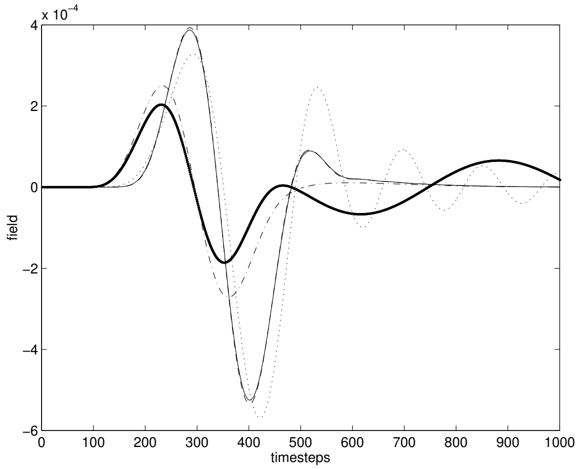

Figure 3. Different pulse distortion for different frequencies of the Lorentz poles. The center frequency of the exciting pulse is 1 GHz. The Lorentz media have the Lorentz frequencies (ω_1 and ω_2) (i) 100 times (dashed line), (ii) 10 times (dotted line), (iii) same (dashed-dot line), and (iii) 0.1 time (heavy solid line) those of Figure 1.

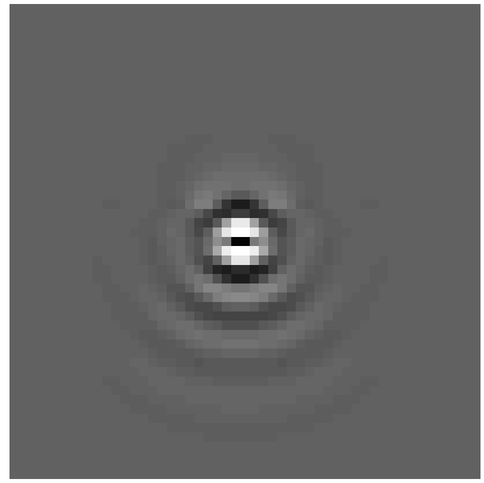

Figure 4. A snapshot of the field profile at 1,000 time steps. No reflection and instability are visible from the edge of the simulation region.

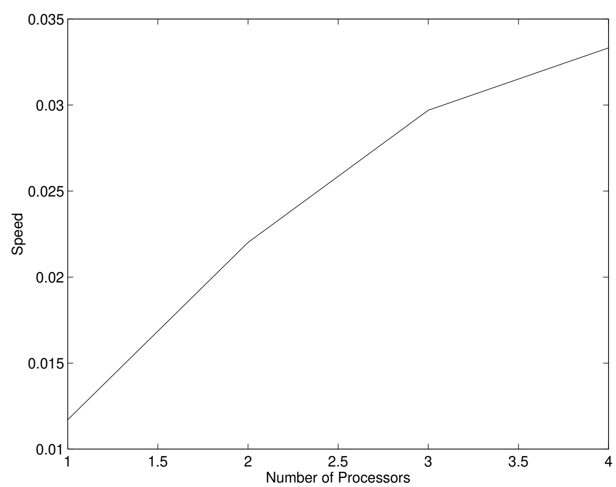

Figure 5. Speedup of the code for 100 time steps for different number of processors on a SGI Power Challenge Array. Linear speedup is observed for a small number of processors, but performance deteriotes as the number of processors increases.